The Astrophysical Journal, 680:809–815, 2008 June 10

PHENOMENOLOGY OF TURBULENT DYNAMO GROWTH AND SATURATION

Rodion Stepanov
Institute of Continuous Media Mechanics, Korolyov 1, 614013 Perm, Russia; rodion@icmm.ru

and

Franck Plunian
Laboratoire de Géophysique Interne et Tectonophysique, Université Joseph Fourier, CNRS, Maison des Géosciences, B.P. 53, 38041 Grenoble Cedex 9, France; Franck.Plunian@ujf-grenoble.fr
Received 2007 October 30; accepted 2008 February 22

ABSTRACT

With a nonlocal shell model of magnetohydrodynamic turbulence we investigate numerically the turbulent dynamo action for low and high magnetic Prandtl numbers (Pr_m). The results obtained in the kinematic regime and along the way to dynamo saturation are understood in terms of a phenomenological approach based on the local ($\mathrm{Pr}_m \ll 1$) or nonlocal ($\mathrm{Pr}_m \gg 1$) nature of the energy transfers. In both cases, the magnetic energy grows at a small scale and saturates as an inverse "cascade."

Subject headings: magnetic fields — methods: numerical — MHD — plasmas — turbulence

Online material: color figures

1. INTRODUCTION

Dynamo action is generally believed to be at the origin of the magnetic field in most astrophysical objects. The conducting fluid which produces the magnetic field is generally strongly turbulent ($\mathrm{Re} \gg 1$) with an extended inertial range. In addition, as it is electrically conducting, the fluid is characterized by the magnetic Prandtl number $\mathrm{Pr}_m = \nu/\eta$, where ν and η are the fluid viscosity and magnetic diffusivity. In a liquid metal as in planetary cores or stellar convective zones $\mathrm{Pr}_m \ll 1$, while in the warm interstellar medium and coronal and cluster plasmas $\mathrm{Pr}_m \gg 1$ (Schekochihin et al. 2002). In direct numerical simulations both conditions, $\mathrm{Re} \gg 1$ and Pr_m much different from unity, are still out of reach of present-day computers. An alternative is to use shell models.

Hydrodynamical shell models are a rough approximation of the Navier-Stokes equations formulated on a discrete set of real wavenumbers $k_n = \lambda^n$, corresponding to a Fourier space divided into shells of logarithmic width λ. They involve (complex) scalar quantities reminiscent of the velocity Fourier components of an isotropic flow. The model satisfies the conservation of both kinetic energy and kinetic helicity when the viscosity is set to zero. It leads to the resolution of a system of ordinary differential equations, requiring much less computing power than the direct numerical simulations of the original equations. It is then possible to run a shell model for realistic values of the viscosity such as $\nu = 10^{-6}$ m^2 s^{-1} (for a review on shell models, see Biferale 2003 and references therein).

The results obtained with shell models are in general agreement with the Kolmogorov phenomenology including intermittency (Leveque & She 1997). First, at any scale k^{-1} lying in the inertial range, the flux rate of kinetic energy is equal to the injection rate of kinetic energy at the forcing scale. This is written as $ku^3(k) \sim \varepsilon$, leading to $u(k) \sim \varepsilon^{1/3}k^{-1/3}$ and to the Kolmogorov spectrum $E(k) \sim \varepsilon^{2/3}k^{-5/3}$. Second, the inertial range is found to extend to the viscous scale k_ν^{-1} which can be evaluated by saying that at this scale the turnover time $k^{-1}u^{-1}$ is comparable to the viscous time $\nu^{-1}k^{-2}$, leading to $k_\nu \sim \varepsilon^{1/4}\nu^{-3/4}$. Third, at low viscosity some deviation from the Kolmogorov power scaling is found due to intermittency. The power scaling of the statistical moments are given by $\langle |u(k)| \rangle^p \sim k^{-\zeta_p}$ with scaling exponents ζ_p deviating from Kolmogorov's mean field theory, $\zeta_p = p/3$. The value of these anomalous scaling exponents given by the shell models compare well with those found in experiments (Leveque & She 1997). Therefore, shell models appear to be a useful tool to study fully developed turbulence at high Reynolds numbers. They are also used in their magnetohydrodynamic (MHD) version to tackle astrophysical issues (Frick et al. 2006; Buchlin & Velli 2007; Galtier & Buchlin 2007).

In a previous paper (Plunian & Stepanov 2007, hereafter PS07), we introduced a nonlocal shell model which is not only in agreement with the previous features of turbulence but in addition gives an appropriate slope of the infrared spectrum in freely decaying turbulence (which is not the case of the local shell models described in Biferale 2003). The MHD version of this model, also introduced in PS07, permits one to study turbulent dynamo action for arbitrary low or high values of Pr_m. In PS07 we calculated the energy transfer functions of the MHD system in a (statistically stationary) saturated state. We found that for $\mathrm{Pr}_m \leq 1$ the energy transfers are mainly local, eventually strengthening our previous results obtained with a local shell model of MHD turbulence (Stepanov & Plunian 2006). For $\mathrm{Pr}_m \gg 1$ the dominant transfers are also mainly local except the ones from the flow scales lying in the inertial range to the magnetic scales smaller than the viscous scale. In that case, the use of a nonlocal model is definitely necessary.

Here, our goal is to describe the transient properties of the turbulent dynamo, namely, the kinematic regime during which the magnetic energy grows exponentially, and the route to saturation, starting when the kinematic regime stops and ending when a (statistically stationary) saturated state is reached. For that, it is not sufficient to make time averages as we did in PS07 when studying the saturated dynamo states. Indeed, the transient properties we are interested in are, by definition, not statistically stationary. Then instead of time averages we have made ensemble averages over $M = 12 \times 10^3$ independent realizations. The initial

conditions have the same energy but random phases. In addition, the forcing also has a random phase in time (therefore different from one realization to the other). Then the results between two realizations are different. After every $t_0 = 10^{-2}$ unit of time we freeze the calculation. For each shell we average the magnetic and kinetic energy over the M realizations without modifying the phases of the magnetic, kinetic, and forcing quantities in order to keep the randomness between every realization. All the calculations were done for $N = 60$ shells, corresponding to more than 12 decades. We have clear numerical evidence that the results obtained with our averaging method are identical to the ones obtained with one run, but much less noisy. Then it is possible to derive values of the growth rate versus time with our method in a much more accurate way than with only one run. Before presenting the results (§§ 3 and 4 for low and high Pr_m) we briefly describe in § 2 the shell model (previously introduced in PS07).

2. THE NONLOCAL SHELL MODEL

The model is defined by the following set of equations,

$$\dot{U}_n = ik_n[Q_n(U,U,a) - Q_n(B,B,a)] - \nu k_n^2 U_n + F_n, \quad (1)$$

$$\dot{B}_n = ik_n[Q_n(U,B,b) - Q_n(B,U,b)] - \eta k_n^2 B_n, \quad (2)$$

where

$$Q_n(X,Y,c) = \sum_{m=1}^{N} T_m(c_m^1 X_{n+m}^* Y_{n+m+1} + c_m^2 X_{n-m}^* Y_{n+1} + c_m^3 X_{n-m-1} Y_{n-1}) \quad (3)$$

represents the nonlinear transfer rates and F_n represents the turbulence forcing applied at shell $n = 0$. Equations (1) and (2) are dimensional equations, B_n being given in units of an Alfvén velocity, the viscosity ν, and magnetic diffusivity η in $\mathrm{m}^2\ \mathrm{s}^{-1}$. As explained in PS07, an optimum shell spacing is the golden number $\lambda = (1 + \sqrt{5})/2$.

For $N = 1$ in equation (3), we recognize the local Sabra model (L'vov et al. 1998). The additional nonlocal interactions for $N \geq 2$ correspond to all other possible triad interactions except the ones involving two identical scales. Expressions for the kinetic energy and helicity E_U and H_U, magnetic energy and helicity E_B and H_B, and cross helicity H_C are given by

$$E_U = \sum_n E_U(n), \quad E_U(n) = \frac{1}{2}|U_n|^2,$$

$$H_U = \sum_n H_U(n), \quad H_U(n) = \frac{1}{2}(-1)^n k_n |U_n|^2, \quad (4)$$

$$E_B = \sum_n E_B(n), \quad E_B(n) = \frac{1}{2}|B_n|^2,$$

$$H_B = \sum_n H_B(n), \quad H_B(n) = \frac{1}{2}(-1)^n k_n^{-1} |B_n|^2, \quad (5)$$

$$H_C = \sum_n H_C(n), \quad H_C(n) = \frac{1}{2}\left(U_n B_n^* + B_n U_n^*\right). \quad (6)$$

In the inviscid and nonresistive limit ($\nu = \eta = 0$), the total energy $E = E_U + E_B$, magnetic helicity, and cross helicity must be conserved ($\dot{E} = \dot{H}_B = \dot{H}_C = 0$). This implies the following expression for the coefficients a_m^i and b_m^i,

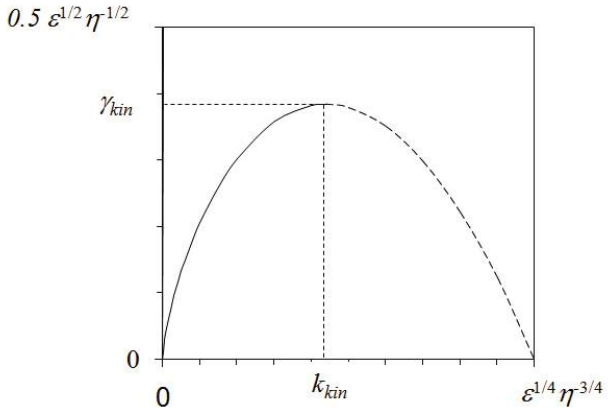

FIG. 1.—Growth rate spectrum $\gamma(k)$ produced by $u(k)$ lying in the inertial range.

$$a_m^1 = k_m + k_{m+1}, \quad a_m^2 = \frac{-k_{m+1} - (-1)^m}{k_m}, \quad a_m^3 = \frac{k_m - (-1)^m}{k_{m+1}},$$
$$b_m^1 = (-1)^{m+1}, \quad b_m^2 = 1, \quad b_m^3 = -1. \quad (7)$$

In the case of pure hydrodynamic turbulence (without magnetic field), the coefficients a_m^i derived from the kinetic energy and helicity conservations ($\dot{E}_U = \dot{H}_U = 0$) would lead to the same expression as equation (7). The coefficients T_m are free parameters depending on m only, which we choose to be of the form $T_m = k_{m-1}^{\alpha}/\lambda(\lambda + 1)$. Further characteristics of the model and results can be found in PS07. In particular, the role of the nonlocality parameter α has been investigated. It is indeed the only free parameter left in the model that cannot be theoretically constrained.

In PS07 we found that taking $\alpha = -5/2$ permits one to describe accurately the infrared hydrodynamic spectrum in freely decaying turbulence. Keeping this value of α in the MHD system for $\mathrm{Pr}_m \leq 1$, we found that the dominant energy transfers are mainly local.

On the other hand, for $\mathrm{Pr}_m \gg 1$, in order to describe properly the nonlocal energy transfer from the flow scales lying in the inertial range to the magnetic scales smaller than the viscous scale, the results obtained in PS07 suggest taking a parameter α corresponding to stronger nonlocal transfers than those obtained for $\alpha = -5/2$. A phenomenological justification of the choice $\alpha = -1$ will be given in § 4.1. It can be also understood as a way to mimic in our (isotropic) model the strongly anisotropic small-scale magnetic turbulence. It is worth mentioning here that taking $\alpha = -1$ does not affect too much the energy transfers involving the magnetic scales lying in the inertial range, which remain mainly local.

3. LOW-Pr_m DYNAMO ACTION

3.1. *Kinematic Regime*

At low Pr_m, as shown in PS07, the energy transfers responsible for the generation of the magnetic energy from the kinetic energy are mainly local, and the flow scales producing the largest magnetic growth rate lie in the inertial range. A phenomenological

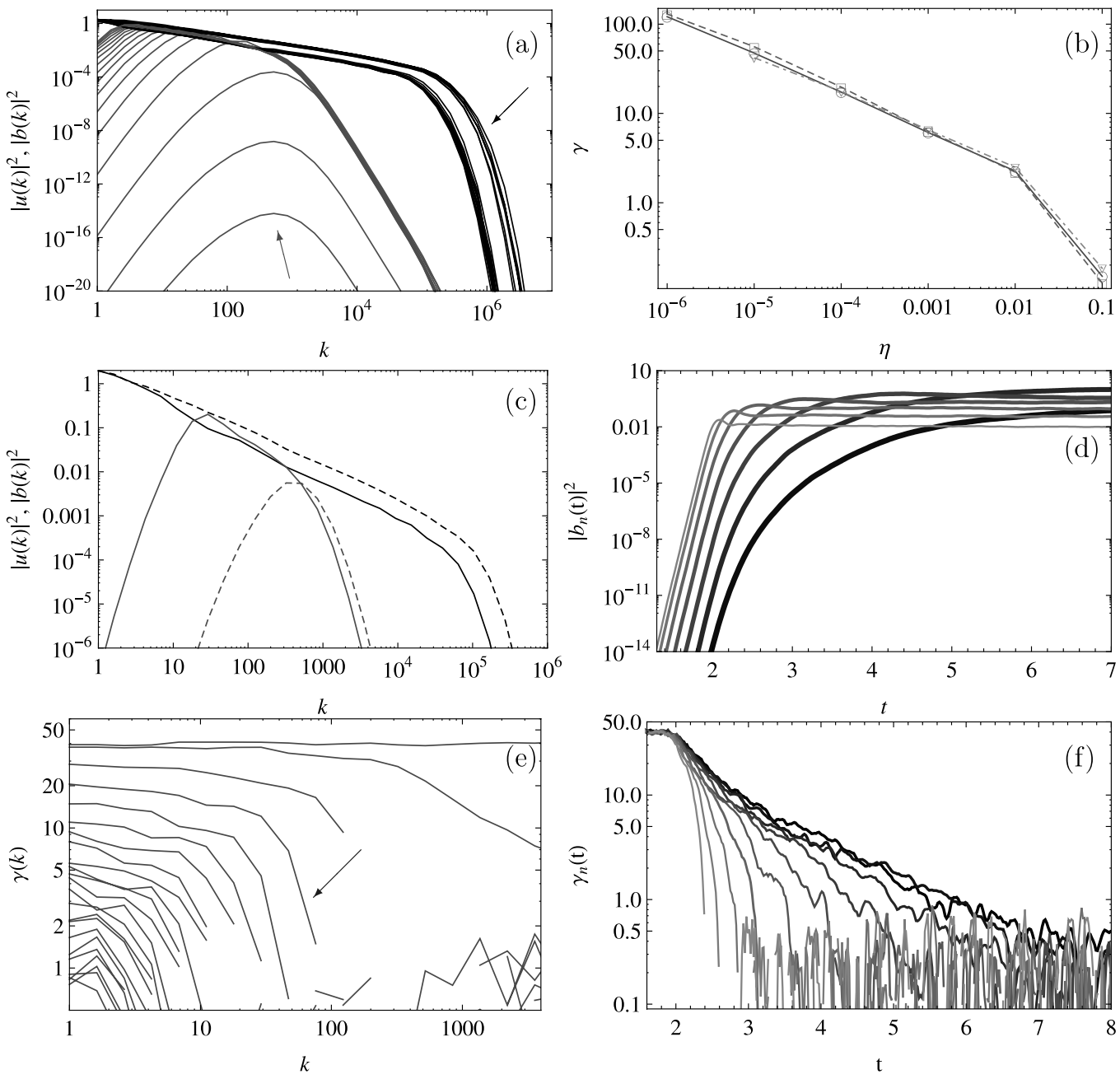

FIG. 2.—Low–magnetic Prandtl number regime $\mathrm{Pr}_m \ll 1$. In all panels except (*b*), $\nu = 10^{-7}$ m^2 s^{-1} and $\eta = 10^{-4}$ m^2 s^{-1}. In (*a*) and (*c*), $|u(k,t)|^2$ (*black curves*) and $|b(k,t)|^2$ (*gray curves*) are plotted vs. k at different times. In (*a*) the arrows give the direction of growing time. In (*c*) the dashed and solid curves correspond to plots at different times, the dashed curves being antecedent. In (*d*) $|b(k,t)|^2$ is plotted vs. time for several values of k. The thickest (and darkest) curve corresponds to the largest scale. The magnetic energy growth rate $\gamma(k,t)$ is plotted vs. k in (*e*) and vs. t in (*f*). In (*e*) the curves evolve from top to bottom along time (*arrow*). In (*f*) the color scale is identical to (*d*). In (*b*) the growth rate during the kinematic regime is plotted vs. η for several viscosities. [*See the electronic edition of the Journal for a color version of this figure*.]

way to understand it is to write the induction equation at wavenumber k in the form

$$\dot{b}(k) = ku(k)b(k) - \eta k^2 b(k), \tag{8}$$

leading to the following growth rate,

$$\gamma(k) = ku(k) - \eta k^2. \tag{9}$$

Assuming a Kolmogorov spectrum in the flow inertial range, $u(k) = \varepsilon^{1/3}k^{-1/3}$, we find $\gamma(k) = \varepsilon^{1/3}k^{2/3} - \eta k^2$, which is plotted in Figure 1. Equation (9) may be misleading in the sense that it gives the impression that each scale grows independently from the others. Actually, strictly local transfers do not exist, implying, together with the linearity of the induction equation, that in the kinematic regime all magnetic scales grow with the same growth rate $\gamma_{\mathrm{kin}} = \max\gamma(k)$. It occurs at $k_{\mathrm{kin}} = 3^{-3/4}\varepsilon^{1/4}\eta^{-3/4}$ with the value $\gamma_{\mathrm{kin}} = 2/(3\sqrt{3})\varepsilon^{1/2}\eta^{-1/2}$.

The resistive scale k_η^{-1} is the scale for which the shear $ku(k)$ is compensated by the resistive dissipation ηk^2, or equivalently, it is the scale for which $\gamma(k) = 0$. We have $k_\eta = \varepsilon^{1/4}\eta^{-3/4}$ and $k_{\mathrm{kin}} = 0.438k_\eta$.

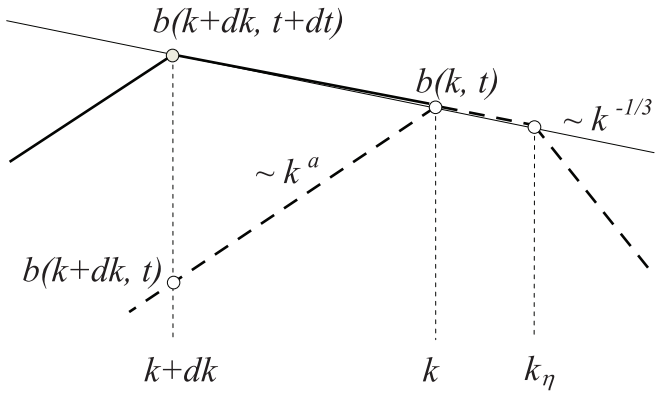

FIG. 3.—Scale by scale saturation mechanism. The dotted (solid) curve represents the $|b|$ spectrum at time t ($t + dt$) in logarithmic coordinates. Here $dt > 0$ and $dk < 0$.

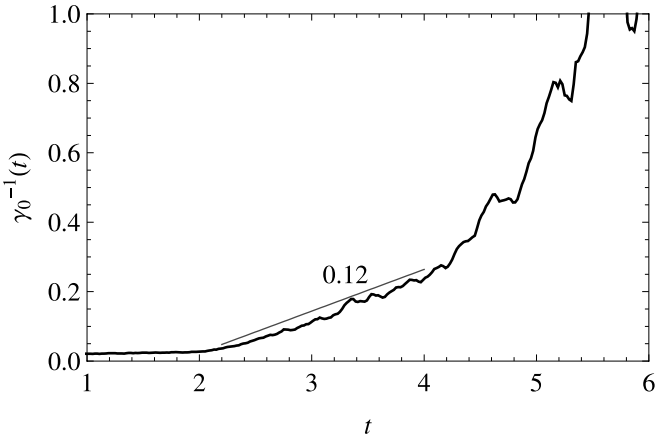

FIG. 4.—Largest scale inverse growth rate γ_0^{-1} vs. t for $\mathrm{Pr}_m = 10^{-3}$. [*See the electronic edition of the Journal for a color version of this figure.*]

Defining a magnetic Reynolds number at wavenumber k by $\mathrm{Re}_m(k) = k^{-1}u(k)/\eta$, we have $\mathrm{Re}_m(k) = \varepsilon^{1/3}k^{-4/3}/\eta$ in the inertial range, and consequently, $\mathrm{Re}_m(k_\eta) = 1$ and $\mathrm{Re}_m(k_{\mathrm{kin}}) = 3$. Comparatively, the magnetic Reynolds number at the forcing scale k_f^{-1} is much larger, scaling as $\mathrm{Re}_m(k_f) \sim \mathrm{Re}_m(k_{\mathrm{kin}})/\eta$. Surprisingly, the kinematic growth rate is given by the small-scale k_{kin}^{-1} for which $\mathrm{Re}_m(k)$ is of order unity and not by the forcing scale k_f^{-1} for which $\mathrm{Re}_m(k)$ is much larger. In addition, k_{kin} and γ_{kin} are viscosity independent in the limit of low Pr_m, suggesting that additional scales in the kinetic inertial range do not change the result. This is also consistent with the fact that the dynamo threshold does not depend on Pr_m in the limit of low Pr_m as shown previously (Ponty et al. 2005; Stepanov & Plunian 2006; Schekochihin et al. 2007).

Coming back to the shell model, as the induction equation is linear in $\boldsymbol{B} = (b_1, b_2, \ldots, b_N)$, where N is the maximum number of shells, we end up with a system of the form $d\boldsymbol{B}/dt = \mathbf{M} \cdot \boldsymbol{B}$, where $\mathbf{M}$ is an $N \times N$ matrix depending on the flow $\boldsymbol{U} = (u_1, u_2, \ldots, u_N)$. During the kinematic regime, the flow $\boldsymbol{U}$ is statistically stationary (the kinematic regime being defined as long as the Lorentz forces are negligible), implying that the system $d\boldsymbol{B}/dt = \mathbf{M} \cdot \boldsymbol{B}$ can be solved as an eigenvalue problem. The eigenvector corresponding to the largest eigenvalue is the one which naturally emerges from the calculation. As explained above, the energy transfers are not strictly local, implying that $\mathbf{M}$ is not diagonal. Then the fastest growing eigenvector should fill all scales. Among the N eigenvalues of the matrix $\mathbf{M}$, the largest one should correspond to γ_{kin} (provided that our phenomenological approach is correct). In addition, the corresponding eigenvector should be peaked at k_{kin}.

In Figure 2*a*, $|u(k)|^2$ (*black curves*) and $|b(k)|^2$ (*gray curves*) are plotted versus k at different times, for $\nu = 10^{-7}$ m^2 s^{-1} and $\eta = 10^{-4}$ m^2 s^{-1}. The kinetic energy satisfies the Kolmogorov scaling $u^2 = \varepsilon^{2/3}k^{-2/3}$ (some deviation occurs due to intermittency as shown in PS07). In the kinematic regime, the magnetic spectrum (Fig. 2*a*, *gray curves*) is peaked at a scale in agreement with k_{kin} and grows exponentially with the same growth rate at all scales as shown in Figure 2*d*, with a growth rate in agreement with γ_{kin}.

The kinematic growth rate has been calculated for other values of $\mathrm{Pr}_m < 1$. It is plotted versus η in Figure 2*b* for three viscosities ($\nu = 10^{-7}$, 10^{-5}, and 10^{-3} m^2 s^{-1}). It is clear from the overlapping curves that the growth rate does not depend on the viscosity. In addition, the curves show a clear power dependence in η. The above phenomenology tells us that $\gamma_{\mathrm{kin}} \sim \eta^r$ with $r = -0.5$. Instead, we find from Figure 2*b* that $r = -0.46$. This apparent discrepancy can be explained from the fact that, as u_n is highly intermittent, we have $u_n \propto k_n^{-\zeta}$ with $\zeta = 0.369$ (instead of the Kolmogorov scaling $\zeta = 1/3$). This new scaling implies $k_{\mathrm{kin}} \sim \eta^{-1/(1+\zeta)}$ and $\gamma_{\mathrm{kin}} \sim \eta^{-(1-\zeta)/(1+\zeta)}$, leading to $r \approx -0.46$.

3.2. *Dynamic Regime*

The kinematic regime ends when the saturation starts. Here, this corresponds to the time when the magnetic energy at wavenumber k_{kin} becomes comparable to the kinetic one $b(k_{\mathrm{kin}}) \approx u(k_{\mathrm{kin}})$. Then due to the Lorentz forces, the magnetic energy at that scale saturates and its growth rate decreases to zero. Meanwhile, the magnetic energy of the next smaller wavenumber (k_{kin}/λ in the shell model) becomes the one with the largest growth rate. Then the wavenumbers $k \le k_{\mathrm{kin}}/\lambda$ continue to grow with the new growth rate $\gamma(k_{\mathrm{kin}}/\lambda)$ until $b(k_{\mathrm{kin}}/\lambda)$ saturates $b(k_{\mathrm{kin}}/\lambda) \approx u(k_{\mathrm{kin}}/\lambda)$. Then the next smaller wavenumber $k_{\mathrm{kin}}/\lambda^2$ becomes the one with the largest growth rate, and successively, all the next smaller wavenumbers change their growth rate in accordance with the growth rate spectrum $\gamma(k)$ given in Figure 1. This saturation mechanism lasts until the smallest wavenumber is saturated. Then an almost equipartition state between both kinetic and magnetic energies is obtained at all scales larger than k_η^{-1}. As stressed in § 5, there is a slight excess of magnetic energy.

Such a scenario is quantitatively illustrated by the mode crossing in Figure 2*d* where the magnetic energy is plotted versus time for several wavenumbers. The way the magnetic wavenumbers get their energy is reversed when compared to the direct hydrodynamic cascade, because it starts at k_{kin} toward smaller wavenumbers. We speak of an inverse "cascade" (Pouquet et al. 1976). It is also illustrated in Figure 2*e* where the magnetic growth rate $\dot{b}(k,t)/b(k,t)$ is plotted versus k at different times. In the kinematic regime, the growth rate is the same at all wavenumbers (*top curve*). Then as time goes on, the plateau of constant growth rate decreases in both intensity and range of involved wavenumbers.

An interesting feature of the route to saturation is shown in Figure 2*c*. The injection rate of kinetic energy ε partly dissipates at the resistive scale k_η^{-1}. A direct consequence is that the viscous scale k_ν^{-1} shifts to larger values during the saturation regime.

Finally, in Figure 2*f* the growth rate $\gamma_n(t) = \dot{b}(k_n,t)/b(k_n,t)$ is plotted versus time for each scale k_n. A signature of the saturation scenario described above is the time evolution of the growth rate at the largest scale (*black curve*). We shall compare it to the following phenomenological description which is sketched schematically in Figure 3.

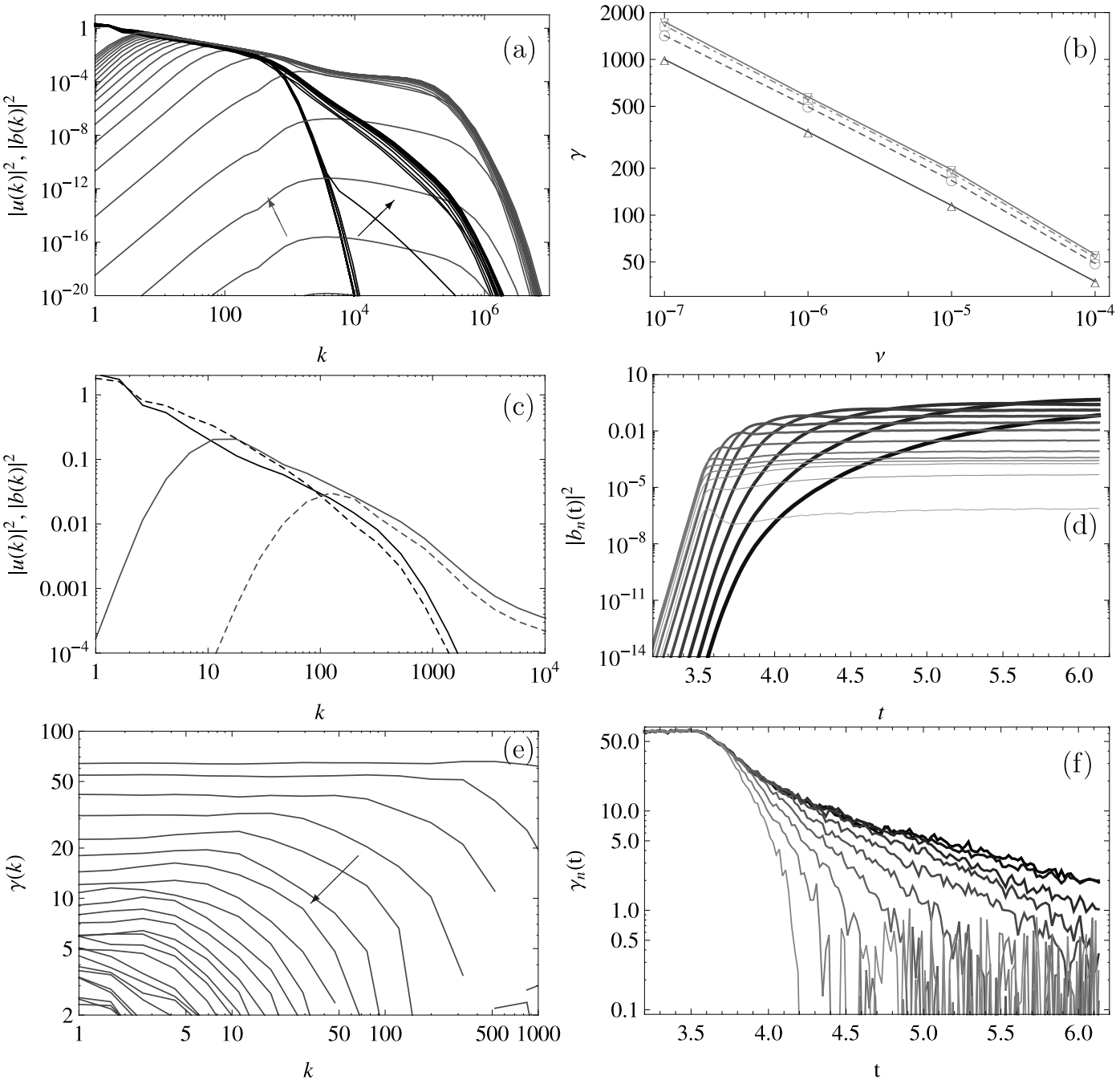

FIG. 5.—High–magnetic Prandtl number regime $\mathrm{Pr}_m \gg 1$. In all figures except (*b*), $\nu = 10^{-4}$ m^2 s^{-1} and $\eta = 10^{-8}$ m^2 s^{-1}. The caption is the same as in Fig. 2 except (*b*) for which the growth rate during the kinematic regime is plotted vs. ν for several diffusivities. [*See the electronic edition of the Journal for a color version of this figure.*]

At time t the magnetic field at wavenumber k reaches its saturation value $b(k,t) = u(k)$. For the left part of the magnetic spectrum scaling as k^a, we have $b(k+dk,t) = b(k,t)(1+dk/k)^a$. Then for $t \le t' \le t+dt$ the magnetic field at scale $k+dk$ (with $dk<0$) grows exponentially as $b(k+dk,t') = b(k+dk,t)\exp[\gamma(k+dk)(t'-t)]$. At time $t' = t+dt$ it reaches its saturation value $b(k+dk,t+dt) = u(k+dk)$. For a Kolmogorov turbulence $u(k+dk) = u(k)(1+dk/k)^{-1/3}$ and assuming that $dk^2 + dt^2 \ll 1$, we finally find

$$dk/dt = -\frac{k\gamma(k)}{(a+1/3)}. \tag{10}$$

From equation (9) and for $k \le k_{\mathrm{kin}}$, a rough approximation of $\gamma(k)$ is $\gamma(k) \sim \gamma_{\mathrm{kin}}(k/k_{\mathrm{kin}})^{2/3}$, leading to

$$\frac{dk}{dt} = -\frac{\gamma_{\mathrm{kin}}}{(a+1/3)k_{\mathrm{kin}}^{2/3}}k^{5/3}. \tag{11}$$

Defining t_0 as the time at which the saturation starts (at $k = k_{\mathrm{kin}}$), we find that the magnetic scale which saturates at subsequent time $t > t_0$ satisfies

$$\frac{k(t)}{k_{\mathrm{kin}}} = \left[1 + \frac{2\gamma_{\mathrm{kin}}}{(1+3a)}(t-t_0)\right]^{-3/2}. \tag{12}$$

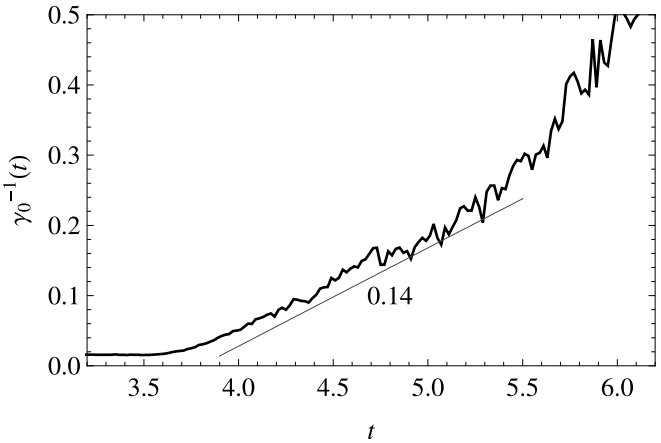

FIG. 6.—Largest scale inverse growth rate γ_0^{-1} vs. t for $\mathrm{Pr}_m = 10^4$. [*See the electronic edition of the Journal for a color version of this figure*.]

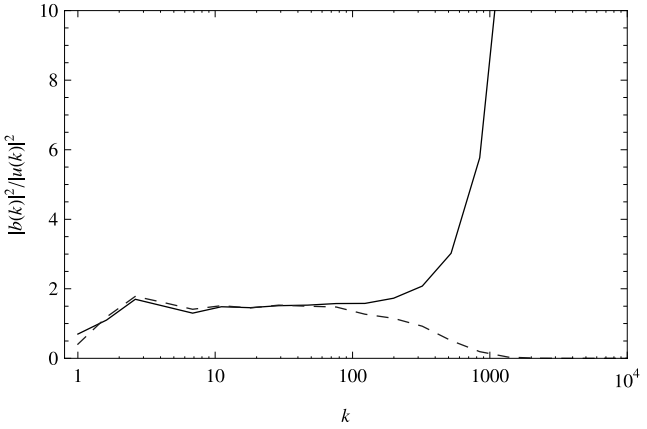

FIG. 7.—Ratio $|b(k)|^2/|u(k)|^2$ plotted vs. k for both cases $\mathrm{Pr}_m = 10^{-3}$ (*dashed curve*) and 10^4 (*solid curve*). [*See the electronic edition of the Journal for a color version of this figure*.]

The growth rate of the largest magnetic scale then satisfies

$$\gamma^{-1}(t) = \gamma_{\mathrm{kin}}^{-1} + \frac{2}{(1+3a)}(t - t_0). \tag{13}$$

This is the signature of the saturation scenario that we want to compare to the shell model results. In the shell model we have $a \approx 2$ (corresponding to an " infrared" spectrum $b^2(k) \sim k^4$ as found, e.g., in Christensson et al. 2001). Therefore, we expect the inverse of the magnetic energy growth rate in shell $n = 0$ to satisfy $(2\gamma)^{-1} = (2\gamma_{\mathrm{kin}})^{-1} + (t - t_0)/7$. In addition, intermittency again changes slightly the result. Indeed for $u \sim k^{-\zeta}$, we find that

$$\gamma^{-1}(t) = \gamma_{\mathrm{kin}}^{-1} + \frac{1-\zeta}{(a+\zeta)}(t - t_0), \tag{14}$$

leading to a slope $d(2\gamma)^{-1}/dt = 0.133$ instead of 1/7 (without intermittency). In Figure 4, $(2\gamma_0)^{-1}$ is plotted versus time. We find indeed a good agreement with the previous expectation, at least for $9 < t < 11$. At subsequent times, the curve diverges because all magnetic wavenumbers are saturated except the two smallest ones ($n = 0, 1$) which continue to be excited by the forcing applied at these wavenumbers. Therefore, the saturation scenario works until the saturation scale becomes close to the forcing scale.

4. HIGH-Pr_m DYNAMO ACTION

4.1. *Kinematic Regime*

At high Pr_m, the resistive scale k_η^{-1} is much smaller than the viscous scale k_ν^{-1}. The flow scale which is responsible for the magnetic growth in the kinematic regime is the one which has the highest shear $ku(k)$. Assuming a Kolmogorov spectrum in the inertial range, we have $ku(k) = \varepsilon^{1/3}k^{2/3}$ which is maximum at the viscous scale k_ν^{-1} [at smaller scales the viscous dissipative range starts and $u(k)$ falls down]. Then the magnetic growth rate in the kinematic regime can be estimated as (Schekochihin et al. 2002, 2004)

$$\gamma = k_\nu u(k_\nu) = (\varepsilon/\nu)^{1/2}. \tag{15}$$

We note that γ depends on the viscosity but not on the diffusivity. The corresponding phenomenologic induction equation is

$$\dot{b}(k) = k_\nu u(k_\nu) b(k) - \eta k^2 b(k) \quad \text{for} \quad k > k_\nu. \tag{16}$$

The resistive scale k_η^{-1} is the scale for which the shear $k_\nu u(k_\nu)$ compensates for the resistive dissipation ηk^2. As at the viscous scale, the shear also compensates for the viscous dissipation, so we have $\eta k_\eta^2 = \nu k_\nu^2$, leading to $k_\eta/k_\nu = \mathrm{Pr}_m^{1/2}$.

From equation (16) we expect a flat spectrum of $|b(k)|^2$ for $k_\nu < k < k_\eta$. In addition, the "infrared" spectrum $k < k_\nu$ is enslaved to the growth of the largest wavenumbers $k > k_\nu$.

Comparing equation (2) with equation (16) we can show that the only way to account for the nonlocal term $k_\nu u(k_\nu) b(k)$ is to take $\alpha = -1$ in the shell model. Indeed, the nonlocal terms involving U_ν and generating magnetic energy $E_B(n)$ with $n \gg n_\nu$ also involve $B_{n\pm1}$ (the subscript ν denotes the viscous shell such that $k_\nu = \lambda^\nu$). The corresponding nonlocal terms in equation (2) are of the form $ik_n(T_{n-\nu}b_{n-\nu}^2 U_\nu^* B_{n+1} + T_{n-\nu-1}b_{n-\nu-1}^3 U_\nu^* B_{n-1})$, which scales as $k_n^{1+\alpha}k_\nu^{-\alpha}$. This scaling is thus equal to k_ν only for $\alpha = -1$.

In Figure 5*a*, $|u(k)|^2$ (*black curves*) and $|b(k)|^2$ (*gray curves*) are plotted versus k at different times, for $\nu = 10^{-4}$ m^2 s^{-1} and $\eta = 10^{-8}$ m^2 s^{-1}. In the kinematic regime, the magnetic spectrum is not completely flat for $k_\nu < k < k_\eta$. This is probably an effect of the additional nonlocal energy transfers involving kinetic scales larger than k_ν^{-1}.

The kinematic growth rate has been calculated for several values of $\mathrm{Pr}_m > 1$. It is plotted versus ν in Figure 5*b* for four values of the magnetic Prandtl number ($\mathrm{Pr}_m = 10, 10^2, 10^3$, and 10^4). For increasing values of Pr_m the curves shift from bottom to top and reach an asymptotic limit showing that the growth rate becomes η-independent at high Pr_m. In addition, the curves show a clear power scaling in ν. The above phenomenology tells us that $\gamma_{\mathrm{kin}} \sim \nu^r$ with $r = -0.5$. Instead, we find from Figure 5*b* that $r = -0.46$. As in the low-Pr_m case, this apparent discrepancy results from the fact that the velocity u_n is intermittent. Then for $u_n \propto k_n^{-\zeta}$ with $\zeta = 0.369$, we find $k_\nu \sim \nu^{-1/(1+\zeta)}$ and $\gamma_{\mathrm{kin}} \sim \nu^{-(1-\zeta)/(1+\zeta)}$, leading to $r \approx -0.46$.

4.2. *Dynamic Regime*

As explained above, during the kinematic regime, the magnetic field $b(k)$ at wavenumber $k > k_\nu$ receives energy from $u(k_\nu)$. It also releases energy to $u(k)$ locally such that the Lorentz force partially compensates for the viscous dissipation. This is visible in Figure 5*a* where in the viscous range for scales $k_\nu < k < k_\eta$, the slope of $|u(k)|^2$ becomes less steep as soon as the magnetic energy is sufficiently large.

TABLE 1

SUMMARY OF THE NUMERICAL VALUES EXPECTED FROM PHENOMENOLOGICAL PREDICTIONS AT LOW Pr_m FOR DIFFERENT VELOCITY SPECTRA $u(k) \sim k^{-\zeta}$

Scaling	ζ	k_{kin}/k_η	$\mathrm{Re}_m(k_{\mathrm{kin}})$	k_{kin}, k_η	k_ν	γ_{kin}	$d(2\gamma)^{-1}/dt$
Phenomenology	...	$[(1-\zeta)/2]^{1/(1+\zeta)}$	$2/(1-\zeta)$	$\eta^{-1/(1+\zeta)}$	$\nu^{-1/(1+\zeta)}$	$\eta^{-(1-\zeta)/(1+\zeta)}$	$(1-\zeta)/(a+\zeta)$
Kolmogorov	1/3	0.439	3	$\eta^{-0.75}$	$\nu^{-0.75}$	$\eta^{-0.5}$	0.143
Intermittency	0.369	0.431	3.17	$\eta^{-0.73}$	$\nu^{-0.73}$	$\eta^{-0.46}$	0.133
Strong rotation	0.5	0.397	4	$\eta^{-0.66}$	$\nu^{-0.66}$	$\eta^{-0.33}$	0.1

At wavenumber $k = k_\nu$ when $|b(k_\nu)|^2 \approx |u(k_\nu)|^2$, the saturation starts and again the saturation occurs from the smaller to larger scales as shown in Figures 5*c*–5*e*. Again, the inverse "cascade" saturation scenario seems to be the relevant one. Indeed, the nonlocal transfers at scales smaller than k_ν are saturated and do not participate in the remaining magnetic growth at larger scales. The results suggest that this remaining growth is mainly governed by local energy transfers within the flow inertial range, similarly to what happens in the small-Pr_m case. Then equations (10)–(14) should stay valid replacing k_{kin} by k_ν and γ_{kin} by $(\varepsilon/\nu)^{1/2}$. In Figure 6, $(2\gamma_0)^{-1}$ is plotted versus time. For $3.5 < t < 7.7$ we find indeed a good agreement with the phenomenological prediction from equation (14). As explained above, at subsequent times the curve diverges as the remaining scales to saturate are larger than the inertial range.

5. DISCUSSION

In the kinematic regime, we found that the magnetic growth rate satisfies $\gamma \sim (\varepsilon/\eta)^{1/2}$ for $\mathrm{Pr}_m \ll 1$ and $\gamma \sim (\varepsilon/\nu)^{1/2}$ for $\mathrm{Pr}_m \gg 1$ and is therefore always fast (Childress & Gilbert 1995). In both cases, this corresponds to a small-scale dynamo (or fluctuation dynamo in the terminology of Schekochihin et al. 2007) in opposition to a large-scale (or mean field) dynamo. At low Pr_m, the magnetic spectrum is peaked at $k = k_{\mathrm{kin}} \approx 0.4k_\eta$, and the energy transfer from kinetic to magnetic is mainly local (as shown in PS07, the nonlocal transfers from small kinetic to large magnetic scales are 20% fewer than the local transfers). At high Pr_m, the magnetic spectrum is almost flat between the viscous and resistive scale, and the energy transfer is mainly nonlocal from $u(k_\nu)$ to $b(k)$ with $k_\nu < k < k_\eta$. In the dynamic regime we found an inverse "cascade" mechanism which explains the route to saturation. The relevance of this mechanism does not depend on Pr_m.

When all magnetic scales are saturated we find that the resulting equilibrium between kinetic and magnetic energy is not an exact equipartition state, showing a slight excess of magnetic energy (Haugen et al. 2003). This is shown in Figure 7, where the ratio $|b(k)|^2/|u(k)|^2$ is plotted versus k, for the values of ν and η corresponding to Figures 2 and 5. For $k_f < k < \min\{k_\nu, k_\eta\}$, the ratio is found to be nearly constant and different from unity ($\approx$1.5) whatever the value of Pr_m. This corresponds to a residual energy (Müller & Grappin 2005) with a Kolmogorov scaling.

Dynamo action is usually found in natural objects with strong rotation. A transition from a Kolmogorov spectrum $E(k) \sim k^{-5/3}$ for weak rotation to $E(k) \sim k^{-2}$ for strong rotation is predicted by weak turbulence theory and is observed in experiments (Baroud et al. 2002, 2003) and numerical simulations (Smith & Waleffe 1999) including shell models (Hattori et al. 2004). It is then of interest to see how the previous phenomenology is changed. At low Pr_m for $u(k) \sim k^{-\zeta}$ with $1/3 \leq \zeta \leq 1/2$, we derive the quantities given in Table 1 and give the numerical values expected for the three scalings, Kolmogorov, intermittent, and strongly rotating. The change of the power scalings from weak to strong rotation should be sufficient to be identified in measurements or numerical calculations. On the other hand, k_{kin}/k_η and $\mathrm{Re}_m(k_{\mathrm{kin}})$ do not change much.

Most of this work was done during the Summer Program on MHD Turbulence at the Université Libre de Bruxelles during 2007 July. The organizers D. Carati and B. Knaepen are warmly thanked as well as the sponsors of this program. R. Stepanov thanks financial support from RFBR grants (07-01-96007 ural and 07-02-00127) and the Russian Federation President grant MK-4338.2007.1. The simulations were performed on the computer cluster of IMM (Ekaterinburg, Russia).

REFERENCES

Baroud, C. N., Plapp, B. B., She, Z.-S., & Swinney, H. L. 2002, Phys. Rev. Lett., 88, 114501
———. 2003, Phys. Fluids, 15, 2091
Biferale, L. 2003, Annu. Rev. Fluid Mech., 35, 441
Buchlin, E., & Velli, M. 2007, ApJ, 662, 701
Childress, S., & Gilbert, A. 1995, Stretch, Twist, Fold: The Fast Dynamo (Berlin: Springer)
Christensson, M., Hindmarsh, M., & Brandenburg, A. 2001, Phys. Rev. E, 64, 056405
Frick, P., Stepanov, R., & Sokoloff, D. 2006, Phys. Rev. E, 74, 066310
Galtier, S., & Buchlin, E. 2007, ApJ, 656, 560
Hattori, Y., Rubinstein, R., & Ishizawa, A. 2004, Phys. Rev. E, 70, 046311
Haugen, N. E. L., Brandenburg, A., & Dobler, W. 2003, ApJ, 597, L141
Leveque, E., & She, Z.-S. 1997, Phys. Rev. E, 55, 2789
L'vov, V., Podivilov, E., Pomlyalov, A., Procaccia, I., & Vandembroucq, D. 1998, Phys. Rev. E, 58, 1811
Müller, W.-C., & Grappin, R. 2005, Phys. Rev. Lett., 95, 114502
Plunian, F., & Stepanov, R. 2007, New J. Phys., 9, 294 (PS07)
Ponty, Y., Mininni, P. D., Montgomery, D. C., Pinton, J.-F., Politano, H., & Pouquet, A. 2005, Phys. Rev. Lett., 94, 164502
Pouquet, A., Frisch, U., & Léorat, J. 1976, J. Fluid Mech., 77, 321
Schekochihin, A. A., Cowley, S. C., Hammett, G. W., Maron, J. L., & McWilliams, J. C. 2002, New J. Phys., 4, 84
Schekochihin, A. A., Cowley, S. C., Taylor, S. F., Maron, J. L., & McWilliams, J. C. 2004, ApJ, 612, 276
Schekochihin, A. A., Iskakov, A. B., Cowley, S. C., McWilliams, J. C., Proctor, M. R. E., & Yousef, T. A. 2007, New J. Phys., 9, 300
Smith, L. M., & Waleffe, F. 1999, Phys. Fluids, 11, 1906
Stepanov, S., & Plunian, F. 2006, J. Turbulence, 7, 39